Hindawi Publishing Corporation
International Journal of Photoenergy
Volume 2014, Article ID 478428, 8 pages
http://dx.doi.org/10.1155/2014/478428

Research Article

Effect of Electrodeposition Potential on Composition of $CuIn_{1-x}Ga_xSe_2$ Absorber Layer for Solar Cell by One-Step Electrodeposition

Rui-Wei You,[1] Kar-Kit Lew,[1] and Yen-Pei Fu[1,2]

[1] *Department of Materials Science and Engineering, National Dong Hwa University, Shoufeng, Hualien 97401, Taiwan*
[2] *Nanotechnology Research Center, National Dong Hwa University, Shoufeng, Hualien 97401, Taiwan*

Correspondence should be addressed to Yen-Pei Fu; d887503@alumni.nthu.edu.tw

Received 3 March 2014; Revised 6 June 2014; Accepted 10 June 2014; Published 14 July 2014

Academic Editor: Ho Chang

CIGS polycrystalline thin films were successfully fabricated by one-step cathodic electrodeposition on Mo-coated glass. In this study, we applied a galvanometry mode with three-electrode potentiostatic systems to produce a constant concentration electroplating solution, which were composed of $CuCl_2$, $InCl_3$, $GaCl_3$, and SeO_2. Then these as-electrodeposited films were annealed in argon atmosphere and characterized by X-ray diffraction. The results revealed that annealing treatment significantly improved the crystallinity of electrodeposited films and formed CIGS chalcopyrite structure, but at low applied deposition voltage (−950 mV versus SCE) there appeared second phase. The cross-section morphology revealed that applied voltage at −1350 mV versus SCE has uniform deposition, and higher applied voltage made grain more unobvious. The deposition rate and current density are proportional to deposition potential, and hydrogen was generated apparently when applying potential beyond −1750 mV versus SCE. It was found that the CIGS compound did not match exact stoichiometry of $Cu:In:Ga:Se = 1:x:(1-x):2$. This result suggests the possibility of controlling the property of thin films by varying the applied potential during electrodeposition.

1. Introduction

$CuInSe_2$ (CIS) and Cu(In, Ga)Se_2 (CIGS) to be candidate materials as absorber material for the thin film photovoltaic device are popular because of high optical absorption and direct band gap. We present that the optimum band gap for solar cell is 1.45 eV. But E_g of $CuInSe_2$ film is near 1.02 eV at room temperature, not exactly located within the best operation area. CIGS cells offer a tunable direct band gap by adjusting the ratio of In to Ga to maximize the absorption of the solar spectrum. To add Ga with appropriate concentration to CIS material could form $CuIn_xGa_{1-x}Se_2$ and adjust the band gap ranges from 1.02 eV (pure $CuInSe_2$) to 1.68 eV (pure $CuGaSe_2$) [1]. This property could be utilized to fabricate multijunction devices for increasing efficiency. Taking CIGS film as an absorber can apparently cause efficiencies of up to 19.5% on a laboratory scale. CIGS cells also have the highest absorption coefficient of any thin film ($\alpha > 105\,cm^{-1}$), which allows for greater than 99% of the incoming photons to be absorbed within the first micron of the material. Cost would be down because of low material requirement. It is estimated that the theoretical efficiency could reach 25% to 30%. After mass production the cost would probably be about US$0.03/W. In sum, a CIGS modules device will have great competition potential for solar energy in the future.

There are different techniques to prepare the CIGS absorber layer including both physical and chemical methods. The main concern for CIGS solar cell is to develop a low-cost and large-scale production technology. It is desirable technically to form the concerned thin film by a simple, safe, and inexpensive procedure. Many researches have reported the fabrication of CIGS by different approaches [2–16]. Xu et al. reported that applying a novel single source

three-stage evaporation process to fabricate CIGS thin film solar cells with a power conversion efficiency of 10.6%. This technique enables the deposition of CIGS thin films using a conventional one-source-at-a-time evaporator and device quality films are formed in situ without selenization [3]. Chen et al. reported one-step fabrication of the chalcopyrite CIGS absorber layer without excess Se supply during/after deposition or postselenization treatments with an efficiency of 10.14% by using pulse DC sputtering route [9]. Later, Chen et al. discussed the characteristics of one-step sputtered CIGS films including compositional, structural, optical, morphological, and electrical properties. For the device fabrication, the authors claimed that Mo back contacts dominated the growth behavior of CIGS films deposited at high temperature [10]. Duchatelet et al. presented new advances on an atmospheric-based deposition process for Cu(In, Ga)Se_2 with an efficiency of 12.4%. The electrodeposition consisted of a Cu-In-Ga mixed oxide/hydroxide layer from an aqueous solution at room temperature, followed by a thermochemical reduction and selenization. This process enables the one-step codeposition of the three elements, from a simple aqueous electrolyte containing nitrate ions as oxygen precursor, with fast growing rates and precise control of composition [11]. Wang et al. reported a novel approach for the fabrication of chalcopyrite $CuIn_xGa_{1-x}Se_2$ thin film solar cells by inkjet printing with a power conversion efficiency of 5.04%. The authors claimed that inkjet printing in atmospheric environment offers an opportunity for the direct patterning of absorber materials at large scale. Moreover, inkjet printing increases the raw material utilization ratio compared to more wasteful vacuum-based deposition techniques [12]. The techniques for the deposition of the CIGS layer can be either vacuum or solution-based methods [13–15]. Although the cell efficiencies obtained from CIGS layer fabricated by the vacuum methods were higher, the cheap and convenient solution-based approaches still attract a lot of research interest as a potential alternative [16].

Among various solution-based methods, electrodeposition is a potentially suitable preparation method for obtaining the low-cost CIGS layer. One-step electrodeposition, especially, has the most various advantages for high throughput and large-area fabrication, because of its low processing cost, the fact that there is no vacuum system needed, its high deposition speed, the fact that there is no use of toxic gases, its low operation temperature, and its simple operation steps. The whole process involves electrodeposition of precursor films of Cu-In-Ga-Se alloy and subsequent recrystallization by thermal annealing at high temperature. The most important part is to optimize deposition parameters and conditions to offer the prospect of achieving stoichiometry. The main emphasis and purpose of this paper focused on details of one-step electrodeposition process. It took depositions' potentials to be process parameters. The goal of this work was to study the effect of the different deposition conditions and treatments used on the structural and morphological properties of CIGS in order to find out the trend of obtaining high quality precursor layers. Grain growth during annealing was observed. The mechanism of film growth and influence of hydrogen generated at cathode are also discussed.

Table 1: Bath composition that used to prepare precursor CIGS thin films by electrodeposition. All chemicals were dissolved in a solution of pH 2 with DI water.

	Bath composition (mM)				
	Cu^{2+}	In^{3+}	Ga^{3+}	Se^{4+}	LiCl
Fixed	12	3.75	6.81	10.8	250

2. Experimental Details

2.1. Thin Film Preparation. One-step electrodeposition was carried out potentiostatically in an aqueous solution containing $CuCl_2$, $InCl_3$, $GaCl_3$, SeO_2, and LiCl; the concentration of each electrolyte is shown in Table 1. No stirring was employed during deposition in first cases; then follow-up cases are under stirring with the velocity using a magnetic bar to improve the uniformity of the deposited sample during deposition (to protect the sample from a bubble generated under the electrolyte solution). The solution temperature was under room temperature without heating and recirculation. Diluted HCl was added drop by drop to adjust the pH of the solution to be between 1.9 and 2.0. It used a classical three-electrode potential static device with platinum (Pt) coated titanium gauze as an auxiliary electrode. Saturated calomel electrode (SCE) is to be a reference for measurement of the local potential of the cathode. The working electrode was a 1-μm thick Mo film on a glass substrate (with active deposition area of 1.0 cm^2) deposited by DC sputtering on soda-lime glass. Ultrasonic cleaner cleaned the specimens with deionized water and acetone. Then they were dried in flowing air. The electrodeposition was controlled using an EG&G Mod. 263 Potentiostat/Galvanostat. To minimize the experimental error, electrodeposition was conducted under the same conditions (concentration of the electrolyte, pH of solution, supporting electrolyte, sample size, and magnetic stirring), except for applied bias. The applied potential was varied from −1950 mV to −950 mV versus SCE [17]. During electrodepositing the current variation was recorded. After electrodeposition precursor thin films were annealed in a tube furnace for 1 hour in Ar atmosphere at 400°C to form CIGS without oxidation and to improve their crystalline properties.

2.2. Thin Film Characterization. The specimens are characterized X-ray diffraction (XRD) by X-ray Diffractometer Rigaku using Cu K_α radiation ($\lambda = 1.54$ Å) to confirm the formation and crystallization of the quaternary compound. The data obtained by XRD was compared with JCPDS file cards in order to determine the phases of the films. The field emission scanning electron microscopy (FESEM) images were used to demonstrate the surface morphology. EDX was done to define compound stoichiometry. The roughness of sample surfaces was detected by atomic force microscopy (AFM).

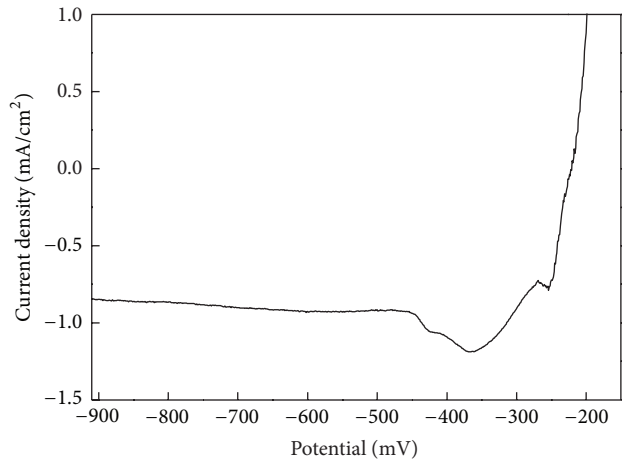

FIGURE 1: Polarization curve was conducted to determine the reduction potentials of each element (scan rate = 1 mV/s).

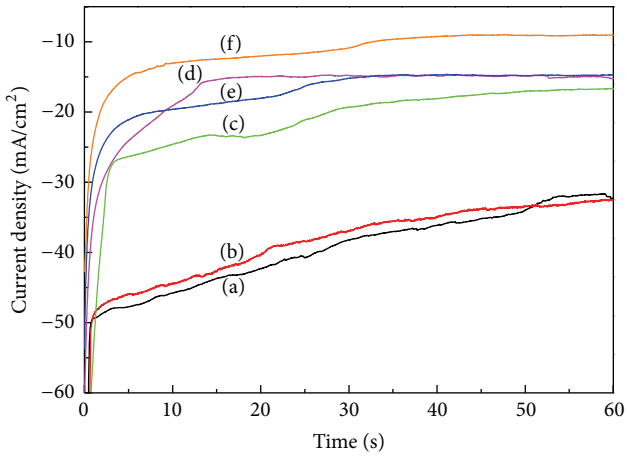

FIGURE 2: *I-T* curve of thin films under different potentials (a) −1950 mV, (b) −1750 mV, (c) −1550 mV, (d) −1350 mV, (e) −1150 mV, and (f) −950 mV.

3. Results and Discussion

The anions of Cu^{2+}, In^{3+}, Ga^{2+}, and $HSeO_3^-$ are believed to exist in the solution. There are reduction reactions which are shown as follows [18, 19]. The optimum reduction potentials of each element listed after chemical formula are standard reduction potentials:

$$Cu^{2+} + 2e^- \longrightarrow Cu \qquad E_0 = +0.337\ V \tag{1}$$

$$In^{3+} + 3e^- \longrightarrow In \qquad E_0 = -0.343\ V \tag{2}$$

$$Ga^{3+} + 3e^- \longrightarrow Ga \qquad E_0 = -0.529\ V \tag{3}$$

$$HSeO_3^- + 5H^+ + 4e^- \longrightarrow Se + 3H_2O \qquad E_0 = +0.740\ V \tag{4}$$

Polarization curve was conducted as in Figure 1. The deviation of these reaction potentials from the theoretically expected values was caused by various factors, such as the concentration of the electrolyte, pH of the solution, used substrate size, supporting electrolyte, and the absence or presence of magnetic stirring [20–23]. Based on theory and [17], the most applicable potential to codeposit these four components should be located between −950 mV versus SCE and −1950 mV versus SCE.

After a round of experiments without stirring, it was found that at higher bias (over −1750 mV versus SCE) a great deal of hydrogen was produced in 10 seconds. Figure 2 shows the *i-t* curves under different potentials. The current density of low bias (below −1350 mV versus SCE) would tend

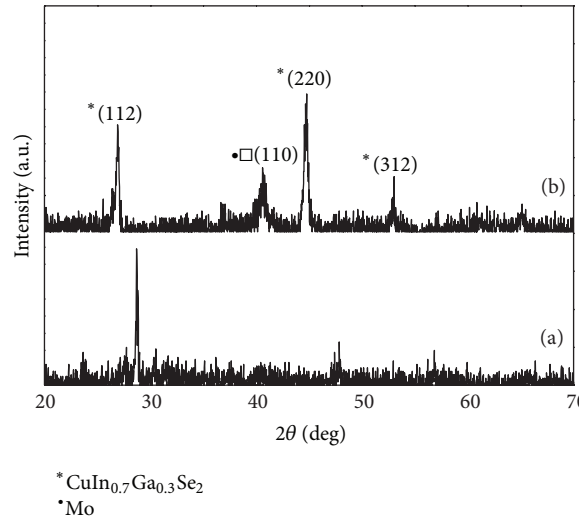

*$CuIn_{0.7}Ga_{0.3}Se_2$
•Mo

FIGURE 3: XRD pattern of thin film deposited under potentials −1350 mV versus SCE for (a) as-annealing and (b) annealing under Ar atmosphere.

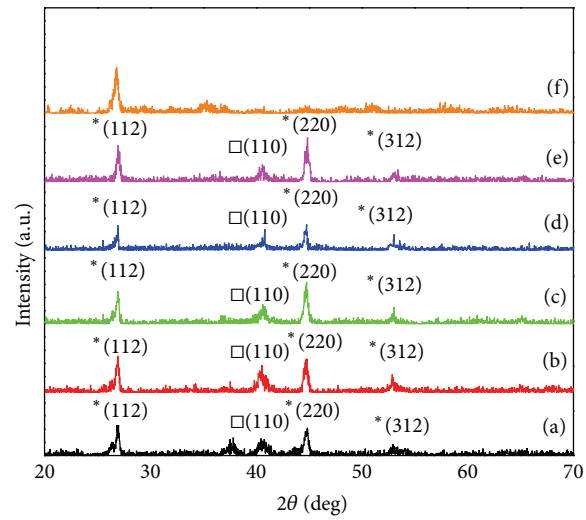

*$CuIn_{0.7}Ga_{0.3}Se_2$
□Mo

FIGURE 4: XRD pattern of thin films deposited under potentials (a) −950 mV, (b) −1150 mV, (c) −1350 mV, (d) −1550 mV, (e) −1750 mV, and (f) −1950 mV.

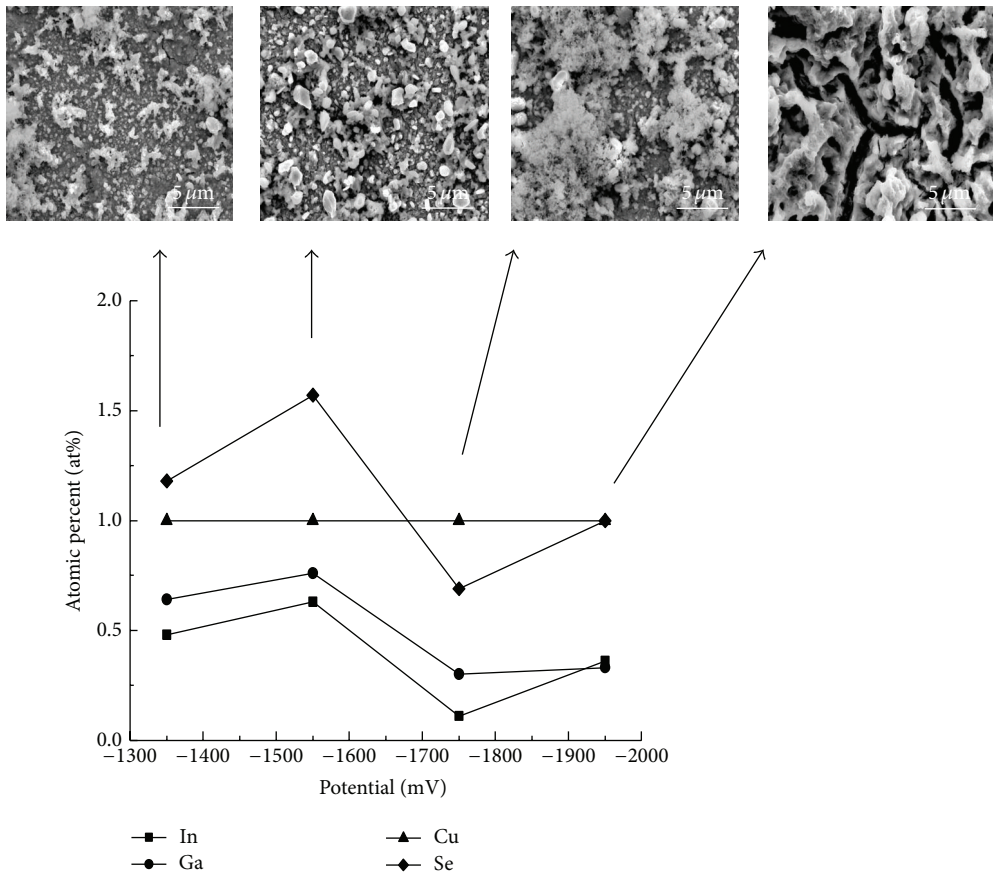

Figure 5: EDS results of CIGS thin films deposited under different potential (normalized to Cu = 1) and its relative surface morphology.

to stabilize and made *i-t* curves horizontal, but for high ones the values of current density were raised with time. Observing the surface after experiments, some areas had no film deposition because of seethe or bubbles adherence. And when presented in aqueous deposition baths, In and Ga deposition efficiencies are limited by H^+ reduction, which cause composition inhomogeneity and pinholes in the film and hence limit the cell efficiencies [18]. To eliminate the effect of hydrogen generation, thereafter electrodeposition was performed by stirring with a magnetic bar.

Figure 3 shows the representative XRD pattern for stoichiometry CIGS samples, annealed and as-annealed, prepared at −1350 mV versus SCE. In the as-deposited sample, pattern just showed a peak at $2\theta = 28.7^\circ$ and the preferred formation of compound is not formed. Furthermore, the uniformity of the thin film is not good without magnetic stirring being used in the deposition procedure. After annealing the sample (400°C, 1 hours, Ar ambient), the quaternary compound, CIGS, is dominantly formed to be chalcopyrite structure in the deposited film. Sharp peaks at $2\theta = 26.9^\circ$, 44.7°, and 53.0° corresponding to the diffraction of the (112), (220), and (312) planes were formed. The 2θ value for (112) plane changed from 28.7° to 26.9°. The phenomenon could be due to the facts that the residual stress would exist in the thin film during electrodeposition processes. The residual stress might lead to lattice anisotropic deformation. The diffraction peak shifted from high to low degree indicated that the lattice spaces increased after annealing. Furthermore, it suggested that the residual stress may be responsible for tensile stress. Figure 4 presents XRD patterns of the samples and thus heat treated after electrodeposition by different deposition potentials. Formation of the main phase of chalcopyrite structure is observed in all samples except −1950 mV one, which had only one preferred orientation at $2\theta = 26.9^\circ$. However, in cases of potentials −950 mV and −1150 mV, there appeared another peak at $2\theta = 37.5^\circ$. But the peak disappeared when applied potential was beyond −1350 mV. It suggested that would have been a secondary phase at lower electrodeposition bias. The peak of secondary phase corresponded to (203) plane of Cu-In alloyed film that annealed to be crystallized to provide the $C_{11}In_9$ phase (stable up to 320°C) [18]. The small positive shift in 2θ value of (112) peak indicated the incorporation of Ga and In sites and hence a decrease in lattice parameter [24].

Figure 5 shows the EDX compositional analysis data, which are normalized to Cu = 1, of the precursor films prepared by electrodeposition at different potentials and corresponded morphologies of top view by SEM. It notes that samples at which −950 mV and −1150 mV were applied are excluded because they did not detect Ga element in thin film. Surface morphology revealed a dendrite surface affected by the electrolyte concentration and duration of deposition which is due to limited ion concentration [18].

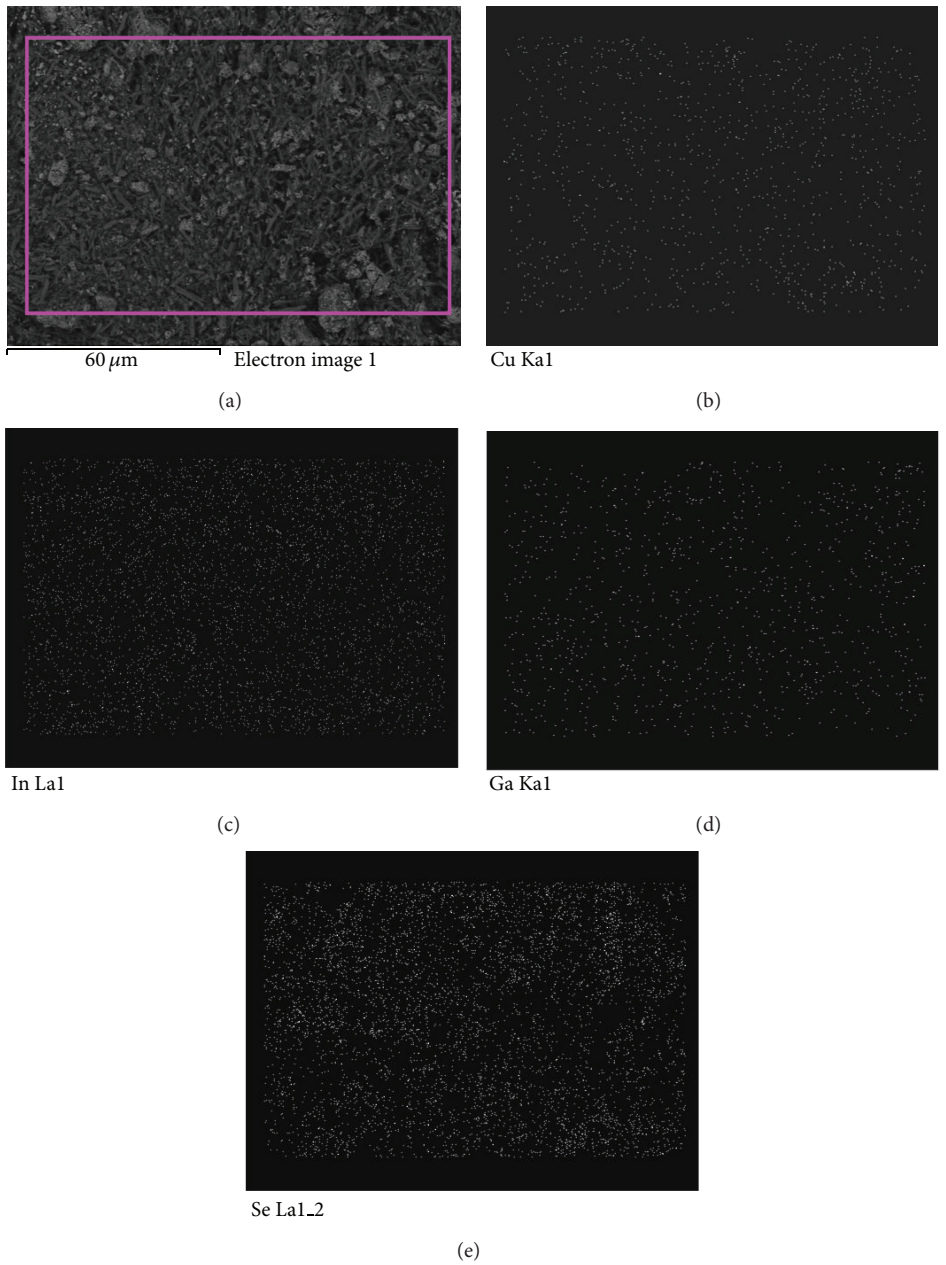

Figure 6: (a) SEM image and corresponding compositional mapping of (b) Cu, (c) In, (d) Ga, and (e) Se of the CIGS film prepared at –1350 mV via electrodeposition.

When electrodeposition process begins, a compact thin film comprising metal elements is formed on the substrate. Based on our group's previous experimental results, it showed that the electrochemical kinetic behavior of the CIGS thin film is strongly influenced by the structure of the electrical double layer existing between the substrate and the electrolyte with different concentrations of Ga^{3+}. With an increase in the electrodeposition time, the kinetic behavior of this electrodeposition system was gradually dominated by the diffusion process rather than the charge-transfer process [25]. In this study, we also observed similar kinetic behavior. With time increasing, the diffusion-controlled reaction gradually dominated the mechanism of the electrodeposition of CIGS layers. The limitation of the electrolyte concentration reaches the substrate, which ions consumed and deposited CIGS. Then, the dendrite structure appeared on the surface [26]. From the SEM images, it could be observed that when more potential was applied, the dendrite size decreased and surface porosity increased. This indicated that the number of nucleation sites in the case of lower deposition potentials is less than that of the higher one. It means that the coalescence of the elements occurs in fewer nucleated sites. Compositional analysis showed that stoichiometry of specimen prepared at –1550 mV was the closest to ratio with $Cu : In : Ga : Se = 1 : (1 - x) : x : 2$. It seems the applied potential and compound stoichiometry are independent, and composition of In, Ga, and Se had

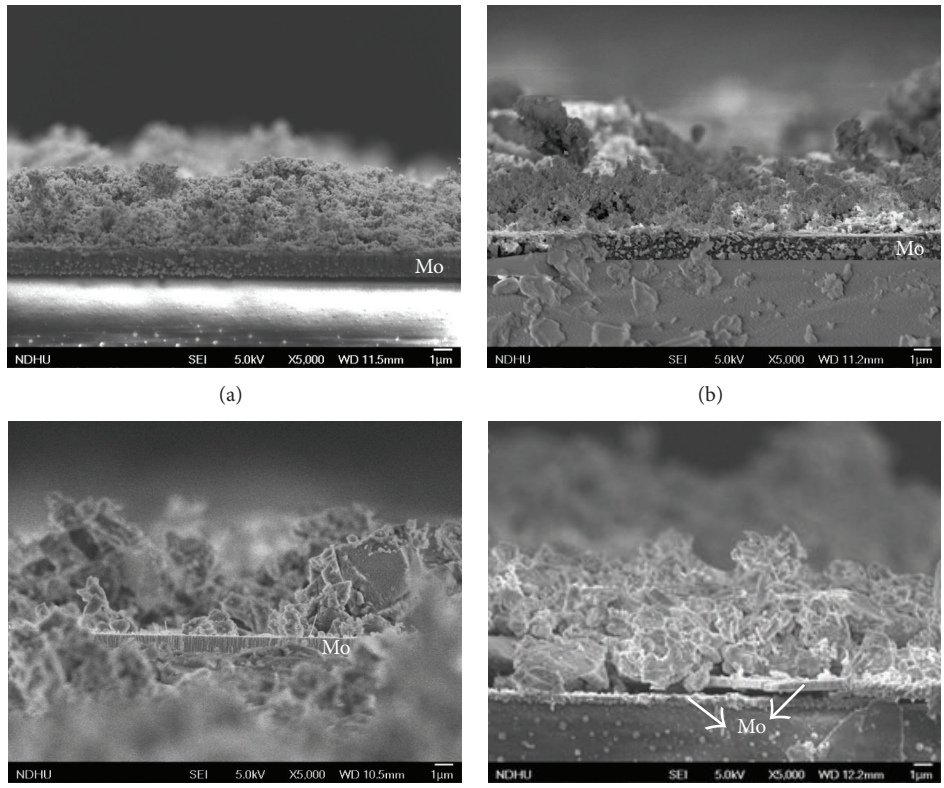

Figure 7: FE-SEM morphology cross-section of thin films deposition at potentials (a) −1350 mV, (b) −1550 mV, (c) −1750 mV, and (d) −1950 mV versus SCE.

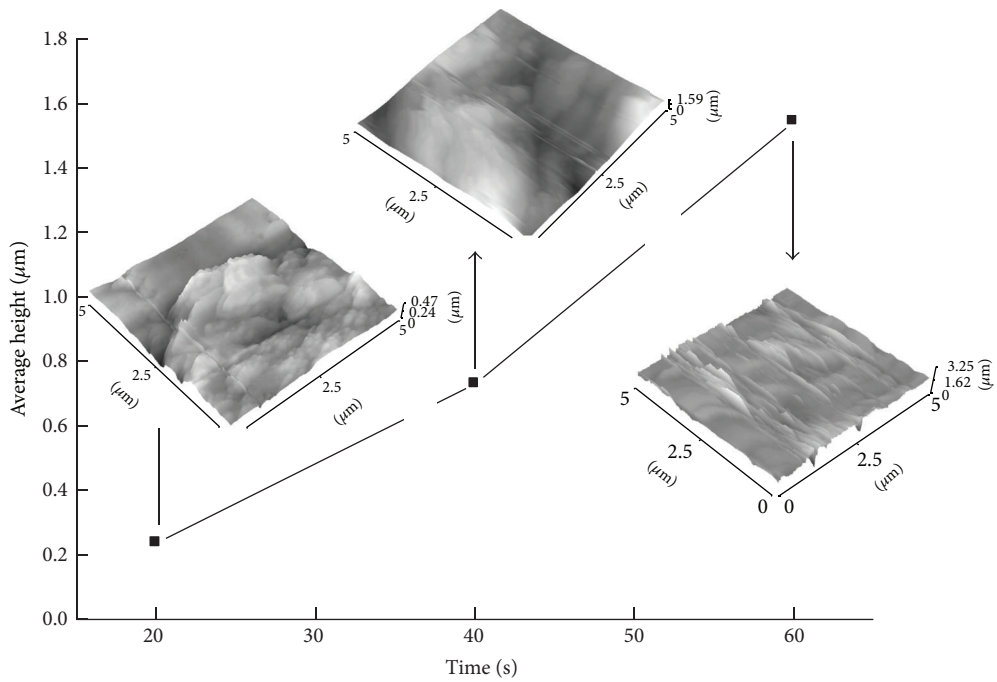

Figure 8: Average height measure by AFM for thin films deposited under potential −1350 mV with different time and its relative surface morphology of AFM image.

Table 2: Roughness measured by AFM for CIGS thin films prepared at electrodeposition potential of −1350 mV.

Electrodeposition time (s)	20	40	60
Roughness average (Ra)	0.0483	0.2516	0.1906
Roughness root mean square (RMS)	0.0606	0.2960	0.2601
Average height maximum	0.2354	0.7289	1.5423
Height maximum	0.4706	1.5879	3.2496

Unit: μm.

same trend with potential when normalized to Cu = 1. To investigate the elemental distribution of CIGS film prepared at −1350 mV via electrodeposition, it was examined by SEM equipped with EDX. The compositional mapping of Cu, In, Ga, and Se exhibited uniform distribution of each element as shown in Figure 6, indicating that no second phases existed on the surface of film.

Figure 7 shows the morphology of the cross-section. As mentioned in the last paragraph, the deposition is limited by the electrolyte concentration that reaches the substrate. At lower applied potential, the metal ions in the bath were consumed slower and diffused more sufficiently than with higher applied potential conduction. Deposit film prepared at −1350 mV was uniform and orderly. The bottom part of −1550 mV cross-section is dense and compact, but with deposition time increasing, the follow-up deposit would become less smooth because of the effect of point discharge and diffusion. Even at −1750 mV and −1950 mV samples, some areas of Mo substrate were rarely deposited and some areas had masses of deposition. Table 2 shows the roughness compared with different deposition time measured by AFM. The roughness root mean square (RMS) and roughness average (Ra) values varied significantly between 20 seconds and 40 seconds; after 40 seconds the roughness varied slightly. It suggested that a large number of atoms did not generate and deposit on substrate surface at initial stage (from 0 to 20 seconds). When certain area of substrate surface had covered the early deposits, it would get advantages to enhance mass transfer process progress with short diffusion distance and high electrical potential gradients. Then the surface would become coarse in this stage (after 40 seconds). Figure 8 shows images and plots of the surface average height. The AFM was used to study the nucleation and development of roughness of the growth of CIGS film. The curve indicated that the roughness increased with deposition time. It was the evidence to explain the surface of thin film deposition influenced by point discharge and diffusion. At first, metal ions at cathode vicinity were depleted in the beginning, but ions cannot supply deposition on time completely. Some areas that had deposits would get advantages, such as short distance for diffusion and high electrical potential gradients due to high charge density. These effects enhanced mass transfer process progress at these knobby parts; then the surface would not worsen uniformly with time. To avoid this behavior, deposition potential, operation time, and stirring should be considered as control parameters. The theoretical thickness of the electrodeposited CIGS layer is determined by the following relationship [27]: $d = (j{\cdot}Mt)/(n{\cdot}F{\cdot}p)$, where j is the current density (mA/cm^2), M is the molecular weight of CIGS (for $CuIn_{0.5}Ga_{0.5}Se_2$ is 315.18 g), t is the time for which the current is passed, p is the density of CIGS, F is the Faraday constant (96500 C), and n is the number of electrons transferred. Based on this equation, one could evaluate the deposited thickness of the CIGS material which was controlled.

4. Conclusions

One-step cathodic electrodeposition of CIGS thin films has been prepared, and the XRD patterns show that annealing treatment improved the crystallization of electrodeposited films and formed CIGS chalcopyrite structure, and at low applied deposition voltage (below −1150 mV versus SCE) there appeared the second phase of Cu-In alloys. The morphology of cross-section displayed that applied voltage at −1350 mV versus SCE has uniform deposition. Ga element could not be detected by EDX when deposition potential is below −1150 mV versus SCE. It was found that the compound did not match exact stoichiometry of $Cu : In : Ga : Se = 1 : x : (1 - x) : 2$. Varying the applied potentials during electrodeposition could control the properties and compounds of CIGS thin film, but the effect was restricted. It should therefore be operated in coordination with electrolyte concentration adjustment in solution to achieve a more ideal composition.

Conflict of Interests

The authors declare that there is no conflict of interests regarding the publication of this paper.

Acknowledgments

The authors would like to thank the National Science Council of Taiwan for financially supporting this research under Contract no. NSC 99-2113-M-259-003 and Nanotechnology Research Center, National Dong Hwa University, for FE-SEM morphology measurements.

References

[1] J. E. Jaffe and A. Zunger, "Theory of the band-gap anomaly in ABC_2 chalcopyrite semiconductors," *Physical Review B*, vol. 29, no. 4, pp. 1882–1906, 1984.

[2] R. N. Bhattacharya, "CIGS-based solar Cells prepared from electrodeposited stacked Cu/In/Ga Layers," *Solar Energy Materials and Solar Cells*, vol. 113, pp. 96–99, 2013.

[3] C. Xu, H. Zhang, J. Parry, S. Perera, G. Long, and H. Zeng, "A single source three-stage evaporation approach to CIGS absorber layer for thin film solar cells," *Solar Energy Materials and Solar Cells*, vol. 117, pp. 357–362, 2013.

[4] N. D. Sang, P. H. Quang, L. T. Tu, and D. T. B. Hop, "Effect of electrodeposition potential on composition and morphology of CIGS absorber thin film," *Bulletin of Materials Science*, vol. 36, no. 4, pp. 735–741, 2013.

[5] S. Nakamura and A. Yamamoto, "Electrodeposited $CuInS_2$-based thin-film solar cells," *Solar Energy Materials and Solar Cells*, vol. 75, no. 1-2, pp. 81–86, 2003.

[6] A. M. Martinez, L. G. Arriaga, A. M. Fernández, and U. Cano, "Band edges determination of $CuInS_2$ thin films prepared by electrodeposition," *Materials Chemistry and Physics*, vol. 88, no. 2-3, pp. 417–420, 2004.

[7] A. M. Fernandez and R. N. Bhattacharya, "Electrodeposition of $CuIn_{1-x}Ga_xSe_2$ precursor films: optimization of film composition and morphology," *Thin Solid Films*, vol. 474, pp. 10–13, 2005.

[8] S. Taunier, J. Sicx-Kurdi, P. P. Grand et al., "$Cu(In,Ga)(S,Se)_2$ solar cells and modules by electrodeposition," *Thin Solid Films*, vol. 480-481, pp. 526–531, 2005.

[9] C. H. Chen, W. C. Shih, C. Y. Chien, C. H. Hsu, Y. H. Wu, and C. H. Lai, "A promising sputtering route for one-step fabrication of chalcopyrite phase $Cu(In,Ga)Se_2$ absorbers without extra Se supply," *Solar Energy Materials and Solar Cells*, vol. 103, pp. 25–29, 2012.

[10] C. Chen, T. Lin, C. Hsu, S. Wei, and C. Lai, "Comprehensive characterization of Cu-rich $Cu(In,Ga)Se_2$ absorbers prepared by one-step sputtering process," *Thin Solid Films*, vol. 535, no. 1, pp. 122–126, 2013.

[11] A. Duchatelet, T. Sidali, N. Loones, G. Savidand, E. Chassaing, and D. Lincot, "12.4% Efficient $Cu(In,Ga)Se_2$ solar cell prepared from one step electrodeposited Cu-In-Ga oxide precursor layer," *Solar Energy Materials and Solar Cells*, vol. 119, pp. 241–245, 2013.

[12] W. Wang, Y. W. Su, and C. H. Chang, "Inkjet printed chalcopyrite CuInxGa_{1-x}Se2 thin film solar cells," *Solar Energy Materials & Solar Cells*, vol. 95, no. 9, pp. 2616–2620, 2011.

[13] A. E. Delahoy, L. Chen, M. Akhtar, B. Sang, and S. Guo, "New technologies for CIGS photovoltaics," *Solar Energy*, vol. 77, no. 6, pp. 785–793, 2004.

[14] M. Kaelin, D. Rudmann, and A. N. Tiwari, "Low cost processing of CIGS thin film solar cells," *Solar Energy*, vol. 77, no. 6, pp. 749–756, 2004.

[15] M. Venkatachalam, M. D. Kannan, N. Muthukumarasamy et al., "Investigations on electron beam evaporated $Cu(In_{0.85}Ga_{0.15})Se_2$ thin film solar cells," *Solar Energy*, vol. 83, no. 9, pp. 1652–1655, 2009.

[16] V. S. Saji, I. H. Choi, and C. W. Lee, "Progress in electrodeposited absorber layer for $CuIn_{(1-x)}Ga_xSe_2$ (CIGS) solar cells," *Solar Energy*, vol. 85, no. 11, pp. 2666–2678, 2011.

[17] T. Yukawa, K. Kuwabara, and K. Koumoto, "Electrodeposition of $CuInS_2$ from aqueous solution (II) electrodeposition of $CuInS_2$ film," *Thin Solid Films*, vol. 286, no. 1-2, pp. 151–153, 1996.

[18] M. Paunovic and M. Schlesinger, *Fundamentals of Electrochemical Deposition*, Wiley-Interscience, Hoboken, NJ, USA, 1998.

[19] R. Caballero, C. Guillén, M. T. Gutiérrez, and C. A. Kaufmann, "$CuIn_{1-x}Ga_xSe_2$-based thin-film solar cells by the selenization of sequentially evaporated metallic layers," *Progress in Photovoltaics: Research and Applications*, vol. 14, no. 2, pp. 145–153, 2006.

[20] M. E. Calixto, P. J. Sebastian, R. N. Bhattacharya, and R. Noufi, "Compositional and optoelectronic properties of CIS and CIGS thin films formed by electrodeposition," *Solar Energy Materials and Solar Cells*, vol. 59, no. 1, pp. 75–84, 1999.

[21] F. Chraibi, M. Fahoume, A. Ennaoui, and J. L. Delplancke, "Influence of citrate ions as complexing agent for electrodeposition of CuInSe2 thin films," *Physica Status Solidi (A) Applied Research*, vol. 186, no. 3, pp. 373–381, 2001.

[22] M. C. F. Oliveira, M. Azevedo, and A. Cunha, "A voltammetric study of the electrodeposition of $CuInSe_2$ in a citrate electrolyte," *Thin Solid Films*, vol. 405, pp. 129–134, 2002.

[23] R. N. Bhattacharya, W. Batchelor, H. Wiesner et al., "14.1% $CuIn_{1-x}Ga_xSe_2$-based photovoltaic cells from electrodeposited precursors," *Journal of the Electrochemical Society*, vol. 145, no. 10, pp. 3435–3440, 1998.

[24] S. M. Babu, A. Ennaoui, and M. C. Lux-Steiner, "Composition and growth procedure-dependent properties of electrodeposited $CuInSe_2$ thin films," *Journal of Crystal Growth*, vol. 275, no. 1-2, pp. e1241–e1246, 2005.

[25] Y. P. Fu, R. W. You, and K. K. Lew, "Electrochemical properties of solid-liquid interfaceof $CuIn_{1-x}Ga_xSe_2$ prepared by electrodeposition with various gallium concentrations," *Journal of the Electrochemical Society*, vol. 156, no. 9, pp. E133–E138, 2009.

[26] S. H. Kang, Y. Kim, D. Choi, and Y. Sung, "Characterization of electrodeposited $CuInSe_2$ (CIS) film," *Electrochimica Acta*, vol. 51, no. 21, pp. 4433–4438, 2006.

[27] A. Parrettam, M. L. Addonizio, A. Agati et al., "Influence of morphology and structure of Cu/In alloys on the properties of $CuInSe_2$," *Japanese Journal of Applied Physics*, vol. 32, pp. 80–83, 1993.